Adiabatic breakdown in a fiber ring resonator

Eyal Buks

Department of Electrical Engineering, Technion, Haifa 32000, Israel

Received August 11, 2005; revised October 2, 2005; accepted October 10, 2005; posted October 18, 2005 (Doc. ID 64016)

I consider a topological transition resulting in an abrupt change by π of the geometric (Berry's) phase occurring in an optical modulator based on a fiber ring resonator. The topological transition, induced by modifying the birefringence along the ring, manifests itself in a narrow resonance in the transmission of the optical modulator. Contrary to the adiabatic case, the condition of critical coupling is not essential to obtain deep modulation of the transmission. Moreover, broadening of the resonance due to the finite linewidth of the optical input is also discussed.

OCIS codes: 060.4080, 080.2740, 350.1370.

1. INTRODUCTION

Optical modulators are devices of great importance for optical communication and other fields. In these devices some external perturbation, e.g., electric or magnetic fields, is employed to modulate the transmission $\mathcal{T}$ between the input and the output optical ports. One of the key properties of an optical modulator is the responsivity, namely, the dependence of $\mathcal{T}$ on the applied perturbation. Enhancing the responsivity is highly desirable in many applications. One way to achieve high responsivity is to employ a resonator configuration with a high-quality factor Q. The multiple back-and-forth reflections occurring in a resonator allow the responsivity to be enhanced in comparison with the case of a reflectionless optical path. Such a ring resonator was considered by Yariv[1,2] and implemented experimentally.[3,4] It was shown that high enhancement is achieved when critical coupling occurs, namely, when the power entering the resonator from the input port equals the outgoing dissipation power. On the other hand, one of the drawbacks of a resonator configuration is the limited optical bandwidth. In some cases the finite linewidth of the optical input $\Delta\omega$ may lead to broadening of the resonance and thus reduce the responsivity. Such broadening can be avoided only when $\Delta\omega/\omega \ll \lambda/QL$, where λ is the wavelength and L is a characteristic length of the resonator.

In this paper we consider a ring resonator similar to the one discussed in Refs. 1 and 2. However, while Refs. 1 and 2 considered the case of polarization-independent evolution, here we study the case of finite birefringence $\kappa(s)$ along the optical path (s is a coordinate along the optical path). The ability to externally control $\kappa(s)$ allows one to employ such a device as an optical modulator. We discuss below the responsivity and other performances of such a modulator and show that such a device may offer some important advantages.

We first consider the case of adiabatic evolution, when κ changes slowly. In this limit the orbital degree of freedom along the fiber is regarded as slow in comparison with the fast evolution of the polarization degree of freedom. In the adiabatic case it is convenient to express the state of polarization (SOP) in the basis of local eigenvectors. In this basis the equations of motion of both polarization amplitudes can be decoupled to the lowest order in the adiabatic expansion. Our analysis is based on a geometric approach to treat evolution of optical polarization that was first employed by Rytov[5] and independently by Pancharatnam.[6] Early experimental demonstrations with optical fibers by Ross,[7] and later by Tomita and Chiao,[8] motivated further extensive theoretical and experimental studies in this field.[9–23]

Next we consider the case of adiabatic breakdown, namely, the transition into the regime where the adiabatic approximation does not hold. In this case the geometric (Berry)[24] phase acquired in a round trip along the ring changes abruptly by π. A similar abrupt change in the geometric phase was discussed before by Bhandari[25–27] and also in Refs. 28 and 29. Experimental demonstrations of this effect employing interferometers were reported in Ref. 30 with a Young's interference setup and in Ref. 31 with a Michelson interferometer. Moreover, a similar adiabatic breakdown was considered in Ref. 32 for the case of spin 1/2 electrons in coherent mesoscopic conductors with a spin-orbit interaction. In the present paper we show that this abrupt change, occurring in the transition between adiabatic and nonadiabatic regimes,[33] can be employed to achieve high responsivity of an optical modulator. As we show below, the width of such a topological transition and, consequently, the responsivity are both determined by the range of validity of the adiabatic approximation. Note, however, that, as is shown in Ref. 34, the linearity of optical modulators imposes in general an upper bound on their responsivity.

Such an optical modulator based on adiabatic breakdown can be implemented in a variety of different configurations. Here I demonstrate these effects by considering a relatively simple example of a modulator based on a fiber ring resonator having both intrinsic and externally applied birefringence. The intrinsic birefringence along the ring in our example is linear. As discussed below, it can be induced using a standard polarization-maintaining fiber that is twisted and tapered to realize the desired birefringence. The externally applied birefringence used for modulation is based on the magneto-optic effect.[35,36] This

effect allows one to induce circular birefringence in the fiber, which is proportional to the Verdet constant characterizing the material and to the component of the applied magnetic field along the direction of propagation. The experimental realization of this proposal is feasible with present-day technology. I employ both analytical and numerical calculations to study the responsivity of the system. Enhanced responsivity is found when we operate in the adiabatic breakdown regime.

2. FIBER RING RESONATOR

Consider a fiber ring resonator as shown in Fig. 1. It consists of a fiber ring coupled to input and output ports using a directional coupler.

The SOP at each point along the fiber is described as a spinor with two components associated with the amplitudes of two orthonormal polarization states. As discussed in Appendixes A and B, we use the local eigenvectors as a basis to express the SOP. The associated amplitudes are $E_{\uparrow}$ and $E_{\downarrow}$, respectively. The directional coupler is assumed to have coupling constants independent of the SOP. Moreover, the coupling is assumed lossless, thus the coupling matrix is unitary:

$$\begin{bmatrix} E_{\uparrow}^{b_1} \\ E_{\uparrow}^{b_2} \\ E_{\downarrow}^{b_1} \\ E_{\downarrow}^{b_2} \end{bmatrix} = \begin{bmatrix} t & r & 0 & 0 \\ -r^* & t^* & 0 & 0 \\ 0 & 0 & t & r \\ 0 & 0 & -r^* & t^* \end{bmatrix} \begin{bmatrix} E_{\uparrow}^{a_1} \\ E_{\uparrow}^{a_2} \\ E_{\downarrow}^{a_1} \\ E_{\downarrow}^{a_2} \end{bmatrix}, \tag{1}$$

where

$$|t|^2 + |r|^2 = 1. \tag{2}$$

Integrating the equation of motion along the ring leads in general to a linear relation between the amplitudes at both ends:

$$\begin{bmatrix} E_{\uparrow}^{a_2} \\ E_{\downarrow}^{a_2} \end{bmatrix} = \hat{M} \begin{bmatrix} E_{\uparrow}^{b_2} \\ E_{\downarrow}^{b_2} \end{bmatrix}, \tag{3}$$

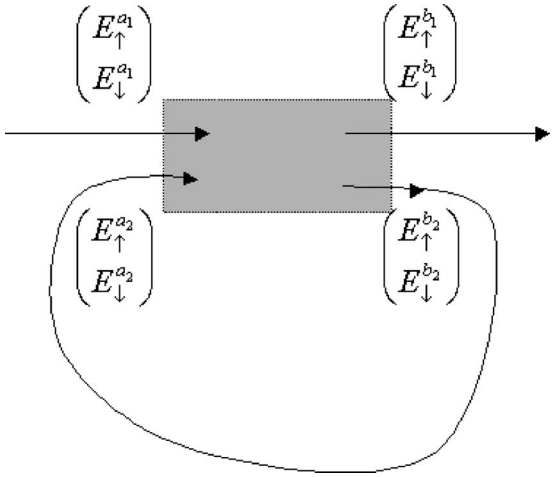

Fig. 1. Fiber ring resonator.

where

$$\hat{M} = \begin{bmatrix} M_{11} & M_{12} \\ M_{21} & M_{22} \end{bmatrix}. \tag{4}$$

Using Eqs. (1)–(3) one can find a linear relation between the amplitudes in the input and output ports of the modulator:

$$\begin{bmatrix} E_{\uparrow}^{b_1} \\ E_{\downarrow}^{b_1} \end{bmatrix} = \hat{S} \begin{bmatrix} E_{\uparrow}^{a_1} \\ E_{\downarrow}^{a_1} \end{bmatrix}, \tag{5}$$

where the matrix $\hat{S}$ is given by

$$\hat{S} = \frac{1 - t\hat{M}^{-1}}{t^* - \hat{M}^{-1}}. \tag{6}$$

Note that if $\hat{M}$ is unitary (namely, $\hat{M}^{-1} = \hat{M}^{\dagger}$) and 2 holds, then, as expected, $\hat{S}$ is unitary as well. Note also that if $\hat{M}$ is diagonal (namely, $M_{12} = M_{21} = 0$), the following holds[1,2]:

$$\hat{S} = \begin{bmatrix} \dfrac{t - M_{11}}{1 - M_{11}t^*} & 0 \\ 0 & \dfrac{t - M_{22}}{1 - M_{22}t^*} \end{bmatrix}. \tag{7}$$

To find the matrix $\hat{M}$ one has to integrate the equation of motion [Eq. (A9)] along the close curve defined by the ring. In the adiabatic limit, to be discussed in Section 3, the solution can be found analytically. In Section 5 the case of adiabatic breakdown is discussed, where both analytical approximations and numerical calculations are employed to integrate the equation of motion [Eq. (A9)].

3. ADIABATIC CASE

In the case where the adiabatic approximation can be applied, the matrix $\hat{M}$ is given by

$$\hat{M} = \begin{bmatrix} \exp(i\delta_{\uparrow}) & 0 \\ 0 & \exp(i\delta_{\downarrow}) \end{bmatrix}, \tag{8}$$

where $\delta_{\uparrow}$ and $\delta_{\downarrow}$ are given by Eqs. (B23) and (B24), respectively.

In the more general case the ring may have internal loss. Assuming that the loss is polarization independent, one has

$$\hat{M} = (1 - \xi_l) \begin{bmatrix} \exp(i\delta_{\uparrow}) & 0 \\ 0 & \exp(i\delta_{\downarrow}) \end{bmatrix}, \tag{9}$$

where $0 \leq \xi_l \leq 1$ is real. Thus using Eq. (7),

$$\frac{E_{\sigma}^{b_1}}{E_{\sigma}^{a_1}} = \frac{t - (1 - \xi_l)\exp(i\delta_{\sigma})}{1 - (1 - \xi_l)\exp(i\delta_{\sigma})t^*}, \tag{10}$$

where $\sigma \in \{\uparrow, \downarrow\}$. Using the notation $t = (1 - \xi_c)\exp(i\theta_t)$, where $0 \leq \xi_c \leq 1$ is real, and $\vartheta = \delta_{\sigma} - \theta_t$, one obtains

$$\frac{E_\sigma^{b_1}}{E_\sigma^{a_1}} = \exp(i\theta_t)\frac{1-\xi_c-(1-\xi_l)\exp(i\vartheta)}{1-(1-\xi_l)(1-\xi_c)\exp(i\vartheta)}. \tag{11}$$

Near resonance, $\vartheta \ll 1$. Moreover, assuming $\xi_l \ll 1$ and $\xi_c \ll 1$, one finds

$$\frac{E_\sigma^{b_1}}{E_\sigma^{a_1}} \simeq \exp(i\theta_t)\frac{\xi_l-\xi_c-i\vartheta}{\xi_l+\xi_c-i\vartheta}. \tag{12}$$

Critical coupling occurs when $\xi_l=\xi_c\equiv\xi$. In this case the transmission amplitude $E_\sigma^{b_1}/E_\sigma^{a_1}$ vanishes at resonance. The transmission probability in this case is given by

$$\mathcal{T}(\vartheta) \simeq \frac{(Q\vartheta)^2}{1+(Q\vartheta)^2}, \tag{13}$$

where $Q=1/2\xi$. Thus high responsivity can be achieved when operating close to a resonance with a high Q factor.

4. BROADENING DUE TO FINITE LINEWIDTH

As was discussed in Section 3, relatively high responsivity can be achieved when operating close to a resonance. However, as we discuss below, the price one has to pay for that is limited bandwidth.

Consider the case where the optical input has some finite linewidth $\Delta\omega$. As a result, the phase factor ϑ will acquire a linewidth given by

$$\Delta\vartheta = 2\pi\frac{\Delta\omega}{\omega}\frac{L}{\lambda}. \tag{14}$$

Consider the case of a polychromatic optical input and assume that the probability distribution of ϑ is Lorenzian with a characteristic width $\Delta\vartheta$:

$$f(\vartheta') = \frac{1}{\pi\Delta\vartheta}\frac{1}{1+\left(\frac{\vartheta'-\vartheta}{\Delta\vartheta}\right)^2}. \tag{15}$$

Averaging with this distribution and relation (13) and employing the residue theorem for evaluating the integral, one finds

$$\bar{\mathcal{T}}(\vartheta) = \int_{-\infty}^{+\infty} d\vartheta' f(\vartheta')\mathcal{T}(\vartheta') = 1-\frac{1}{1+Q\Delta\vartheta}\frac{1}{1+\left(\frac{Q\vartheta}{1+Q\Delta\vartheta}\right)^2}. \tag{16}$$

Thus, for this case, broadening can be avoided only if $Q\Delta\vartheta \ll 1$ or $\Delta\omega/\omega \ll \lambda/QL$.

5. ADIABATIC BREAKDOWN

While in the previous case both adiabatic SOPs are effectively decoupled, we consider now the transition between adiabatic and nonadiabatic regimes.

The birefringence along the fiber ring is described by the vector $\kappa(s)$ (see Appendix A). Consider the case where in some section of the ring $\kappa(s)$ is close to the degeneracy point at the origin $\kappa=0$. In this case a small perturbation applied to $\kappa(s)$ can result in a large change in the geometric phase [see Eqs. (B20) and (B21)]. This can be seen by considering, for example, the case of a planar curve $\kappa(s)$. In this case the solid angle is given by $\Omega=2\pi n$, where n is the winding number of the curve $\kappa(s)$ around the origin. As the curve $\kappa(s)$ crosses the origin at some point, n changes abruptly by one, leading thus to an abrupt change in the geometric phase. Note, however, that near this transition when $|\kappa(s)|$ is small, the adiabatic approximation breaks down and alternative approaches are needed.

As an example for such a transition we consider a ring resonator for which the close curve $\kappa(s)$ has the shape seen in Fig. 2(c) in the unperturbed case. This curve is made of a half-circle section in the 1–3 plane (the linear birefringence plane) and a diameter section along the κ_3 axis crossing the origin. Such a structure can be realized by using a polarization-maintaining fiber and by employing fiber tapering techniques. The half-circle section can be made out of a Möbius-like ring made of the polarization-maintaining fiber. After welding the two ends of the twisted fiber to form the Möbius structure, one can employ tapering techniques to form the diameter section.

The curve $\kappa(s)$ is perturbed by applying a magnetic field on part of the diameter section of the fiber ring. Such

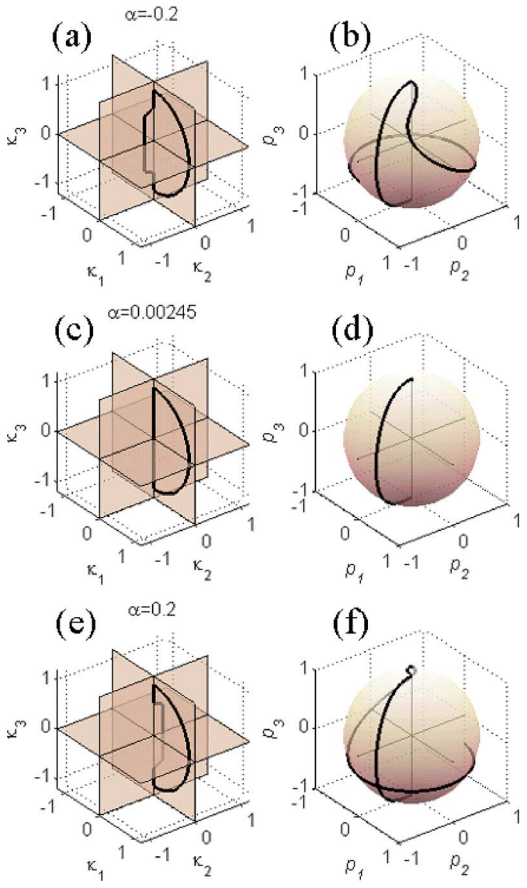

Fig. 2. (Color online) Birefringence $\kappa(s)$ and polarization $\mathbf{P}(s)$ along the fiber ring. Plots (c) and (d) show the unperturbed case; in (a) and (b) the perturbation parameter is $\alpha=-0.2$, and in (e) and (f) $\alpha=0.2$.

a perturbation contributes circular birefringence in the κ_2 direction [see Figs. 2(a) and 2(e)]. The relatively high value of the Verdet constant in common optical fibers allows a significant magneto-optic effect with moderate applied magnetic fields. While the adiabatic approximation totally breaks down in the unperturbed case of Fig. 2(c) when the curve $\kappa(s)$ crosses the origin, the perturbation transforms the system into the regime where adiabaticity holds. As is shown below, the responsivity of the system is relatively high when operating near this transition between the adiabatic and the nonadiabatic regimes.

The half-circle section is analyzed in Appendix C. As can be seen in Fig. 6, the Zener transition probability p_z vanishes for a series of points denoted as Λ_n. In our example we chose Λ to be the first zero of $p_z(\Lambda)$, namely, $\Lambda=\Lambda_1=1.022$. One advantage of choosing one of the zeros of $p_z(\Lambda)$, where p_z obtains a local minimum, is the fact that p_z is only weakly affected by small deviations of $\kappa(s)$ from the ideal half-circle curve. For the parameter γ we chose the value $\gamma=1$. As can be seen from Fig. 2(d), for this choice the evolution along the half-circle section transforms the polarization vector on the Bloch sphere from the pole on the negative P_z axis to the opposite pole on the positive P_z axis. The fiber length of this section is $2\Lambda_1/\gamma$.

The rest of the fiber ring has a birefringence given by $\kappa(s)=\kappa_0(s)+\kappa_1(s)$, where $\kappa_0(s)$ is the unperturbed birefringence forming the diameter section and $\kappa_1(s)$ is the perturbation induced by the magnetic field. The unperturbed part is assumed to be given by

$$\kappa_0(s) = -\left(0,0,\frac{\Lambda_1\gamma^2}{\beta}s\right), \tag{17}$$

where $|s|<\beta/\gamma$. In our numerical example the dimensionless parameter β is given the value $\beta=5$. The perturbation due to the applied magnetic field gives rise to birefringence given by

$$\kappa_1(s) = \left(0,\frac{\alpha}{1+\exp A\left[\left(\frac{\gamma_s}{\beta}\right)^2 - B^2\right]},0\right), \tag{18}$$

where $A=50$ and $B=0.6$ in our numerical example. Thus the magnetic field is applied to a fiber section of length $2B\beta/\gamma$ and drops down to zero abruptly outside this section (due to the large value chosen for the parameter A). The coupling constants in the numerical example are $\xi_c=10^{-2}$ and $\xi_l=10^{-4}$.

The equation of motion along the fiber ring is integrated numerically as described in Appendix A. This allows us to calculate the evolution of the polarization vector on the Bloch sphere [see Figs. 2(b), 2(d), and 2(f)]. The same calculation also yields the matrix $\hat{M}$. The off-diagonal matrix elements allow us to calculate the Zener transition probability $|M_{12}|^2=|M_{21}|^2$ [see Fig. 3(a), solid curve]. The curve shows the gradual transition between the nonadiabatic limit where $|\alpha|\ll 1$ and the adiabatic limit $|\alpha|\gg 1$. An approximated analytical expression for the Zener probability in a similar case where the curve $\kappa(s)$ is an infinite straight line is derived in Appendix C.

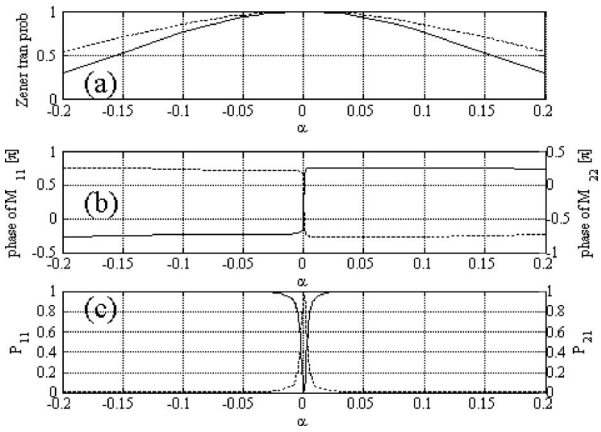

Fig. 3. Dependence on the perturbation amplitude α. (a) Zener transition probability, calculated numerically (solid curve) and estimated using relation (C25). (b) Phase of M_{11} (solid curve) and of M_{22} (dashed curve). (c) Transmission probability into both SOPs, $P_{11}=|S_{11}|^2$ (solid curve) and $P_{21}=|S_{21}|^2$ (dashed curve).

The result in relation (C25) can be used to estimate approximately the Zener transition probability for the present example:

$$p_z = \exp\left(-\frac{\pi\beta\alpha^2}{\Lambda_1\gamma^2}\right). \tag{19}$$

The estimate in Eq. (19) is shown in Fig. 3(a) as a dashed curve. The deviation between the numerical and the analytical results originates mainly because the straight-line section in $\kappa(s)$ is finite while the analytical analysis assumes an infinite straight line. Moreover, the analytical result is expected to hold only in the limit where $|p_z|\ll 1$ as it is evaluated only to the lowest order in the adiabatic expansion.

Figure 3(b) shows the phase of both diagonal matrix elements of $\hat{M}$. In both cases the phase changes abruptly by π near $\alpha=0$. This is originated by the sharp change of the solid angle Ω by 2π near $\alpha=0$ [see Eqs. (B23) and (B24)]. The optical modulator discussed in the present work employs this sharp change to achieve high responsivity.

Figure 3(c) shows the transmission probability into both SOPs, $P_{11}=|S_{11}|^2$ (solid curve) and $P_{21}=|S_{21}|^2$ (dashed curve), of the entire modulator. For both cases, the full width at half-maximum (FWHM) is $\Delta\alpha=5.1\times10^{-3}$.

6. DISCUSSION

As we have seen, the ring resonator can serve as an optical modulator with high responsivity when operated near one of its resonances. Two regimes of operation were considered, the adiabatic and the nonadiabatic. In Subsections 6.A–6.C we compare between both regimes by considering the optical source linewidth, critical coupling, and responsivity.

A. Optical Source Linewidth

In the adiabatic limit, when the equations of motion in the adiabatic basis become decoupled, the only effect of the external perturbation is on the phases acquired along the fiber ring. The dependence of the dynamical phase on

wavelength gives rise to broadening of resonances when one operates with an optical input having a finite linewidth. In the general nonadiabatic regime, however, the external perturbation can affect not only the phase factors but also the SOP as it evolves along the close fiber ring. The later, being wavelength independent, gives rise to a modified dependence on the optical source linewidth.

B. Critical Coupling

In the adiabatic regime full modulation between zero and one of the transmission probability $\mathcal{T}$ is possible only when critical coupling occurs, namely, $\xi_c=\xi_l$, [see relation (12)]. In practice, fulfilling this condition when $\xi_c=\xi_l \ll 1$ is difficult. However, this condition is not essential in the general nonadiabatic case. As can be seen in Fig. 3(c), full modulation is achieved, even though for this example $\xi_c=100\xi_l$.

C. Responsivity

The responsivity of the ring resonator device can be characterized by the FWHM and the height of the resonance near which the device is being operated. As was discussed above, $\Delta\alpha=5.1\times10^{-3}$ for the example presented in Fig. 3. For the same parameters the FWHM of the resonances in the adiabatic regime $|\alpha|\gg1$ can be evaluated using relation (12), yielding $\Delta\alpha=1.7\times10^{-3}$. However, as was discussed above, since the coupling is not critical, the modulation is not full in the adiabatic case. Note that in general the responsivity has an upper bound imposed by the linearity of the system.[34] It can be shown that for both cases, the obtained responsivity is of the same order as the upper bound. A future publication will discuss this point in more detail.

7. SUMMARY

In the present work we study topological transitions in the geometric phase occurring in an optical modulator based on a fiber ring resonator. We find that operating close to the transition can allow relatively high responsivity, even when coupling is not set to be critical. I point out that the geometric phase is independent on the wavelength of the optical input. With optimum design the responsivity can approach the limit set by the linearity of the modulator.[34] Experimental realization of the proposed system, which can be achieved using standard well-established techniques, will allow for the study of topological transitions under well-controlled conditions.

APPENDIX A: STATE OF POLARIZATION EVOLUTION ALONG A FIBER

Consider an optical fiber wound in some spatial curve in space. Let $\mathbf{r}(s)$ be an arc-length parametrization of this curve, namely, the tangent $\hat{\mathbf{s}}=d\mathbf{r}/ds$ is a unit vector. The normal unit vector $\hat{\nu}$ and the curvature κ are defined as $d\hat{\mathbf{s}}/ds=\kappa\hat{\nu}$. One can easily show that $\hat{\nu}\cdot\hat{\mathbf{s}}=0$ by taking the derivative of $\hat{\mathbf{s}}\cdot\hat{\mathbf{s}}=1$ with respect to s. The vectors $\hat{\mathbf{s}}$, $\hat{\nu}$ and the binormal unit vector, defined as $\hat{\mathbf{b}}=\hat{\mathbf{s}}\times\hat{\nu}$, form a local triplet orthonormal coordinate frame known as the Serret–Frenet frame[7,9,37] (see Fig. 4). By taking the derivative of $\hat{\mathbf{s}}\cdot\hat{\nu}=0$ with respect to s, one finds $\hat{\mathbf{s}}\cdot d\hat{\nu}/ds=-\kappa$. Similarly, by taking the derivative of $\hat{\mathbf{b}}\cdot\hat{\nu}=0$ with respect to s, one finds $\hat{\mathbf{b}}\cdot d\hat{\nu}/ds=-\hat{\nu}\cdot d\hat{\mathbf{b}}/ds$. Using the definition $\hat{\mathbf{b}}=\hat{\mathbf{s}}\times\hat{\nu}$, one finds $d\hat{\mathbf{b}}/ds=\hat{\mathbf{s}}\times d\hat{\nu}/ds$. Thus $\hat{\mathbf{s}}\cdot d\hat{\mathbf{b}}/ds=0$. Moreover, by taking the derivative of $\hat{\mathbf{b}}\cdot\hat{\mathbf{b}}=1$ with respect to s, one finds $\hat{\mathbf{b}}\cdot d\hat{\mathbf{b}}/ds=0$. Thus $d\hat{\mathbf{b}}/ds$ is parallel to $\hat{\nu}$. The torsion τ is defined as $d\hat{\mathbf{b}}/ds=-\tau\hat{\nu}$. The above definitions and relations can be summarized as follows:

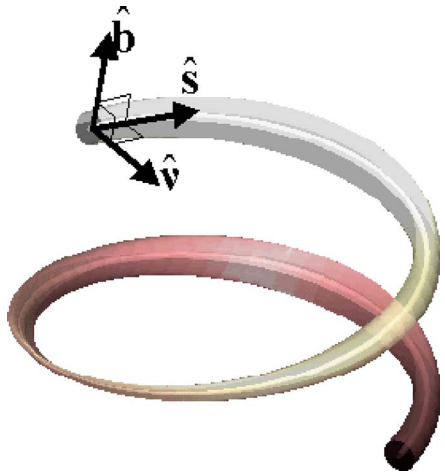

Fig. 4. (Color online) Serret–Frenet frame.

$$\frac{d}{ds}\begin{bmatrix}\hat{\mathbf{s}}\\ \hat{\nu}\\ \hat{\mathbf{b}}\end{bmatrix}=\begin{bmatrix}0 & \kappa & 0\\ -\kappa & 0 & \tau\\ 0 & -\tau & 0\end{bmatrix}\begin{bmatrix}\hat{\mathbf{s}}\\ \hat{\nu}\\ \hat{\mathbf{b}}\end{bmatrix}. \tag{A1}$$

The equation of motion along the optical ray defined by the fiber can be obtained using the transport equation of geometrical optics[5] for the electric field phasor $\mathbf{E}_0$:

$$2(\nabla\psi\cdot\nabla)\mathbf{E}_0+\mathbf{E}_0[\nabla^2\psi-\nabla(\ln\mu)\cdot\nabla\psi]+2[\mathbf{E}_0\cdot\nabla(\ln n)]\nabla\psi=0, \tag{A2}$$

where ψ is the eikonal, n is the index of refraction, and μ is the permeability. We define the unit vector $\hat{\mathbf{e}}_0=\mathbf{E}_0/\sqrt{\mathbf{E}_0\cdot\mathbf{E}_0^*}$ in the direction of $\mathbf{E}_0$. In terms of $\hat{\mathbf{e}}_0$ the transport equation reads

$$\frac{d}{ds}\hat{\mathbf{e}}_0=-\kappa(\hat{\mathbf{e}}_0\cdot\hat{\nu})\hat{\mathbf{s}}. \tag{A3}$$

Expressing the unit vector $\hat{\mathbf{e}}_0$ in the Serret–Frenet frame,

$$\hat{\mathbf{e}}_0=e_\nu\hat{\nu}+e_b\hat{\mathbf{b}}, \tag{A4}$$

one finds using Eq. (A1)

$$\frac{de_\nu}{ds}\hat{\nu}+\frac{de_b}{ds}\hat{\mathbf{b}}+e_\nu(-\kappa\hat{\mathbf{s}}+\tau\hat{\mathbf{b}})-e_b\tau\hat{\nu}=-\kappa e_\nu\hat{\mathbf{s}}. \tag{A5}$$

Thus, using the Dirac ket notation.

$$|e\rangle\doteq\begin{bmatrix}e_\nu\\ e_b\end{bmatrix}, \tag{A6}$$

one finds

$$\frac{\mathrm{d}}{\mathrm{d}s}|e\rangle = i\mathcal{K}_g|e\rangle, \tag{A7}$$

where the geometric birefringence $\mathcal{K}_g$ is given by

$$\mathcal{K}_g = \tau\begin{bmatrix} 0 & -i \\ i & 0 \end{bmatrix}. \tag{A8}$$

Equation (A7) is known as Rytov's law.[5] In the more general case where other birefringence mechanisms are present, the equation of motion reads

$$\frac{\mathrm{d}}{\mathrm{d}s}|e\rangle = i\mathcal{K}|e\rangle, \tag{A9}$$

where $\mathcal{K}=\mathcal{K}_g+\mathcal{K}_f$, and $\mathcal{K}_f$ is the birefringence in the fiber due to the intrinsic structure or to elasto-optic or electro-optic of the magneto-optic effects.

In a lossless fiber the matrix $\mathcal{K}$ is Hermitian. For this case it is convenient to expresses $\mathcal{K}$ as

$$\mathcal{K} = k_0 I + \kappa\cdot\sigma, \tag{A10}$$

where I is the 2 by 2 identity matrix, k_0 is a real scalar, $\kappa=(\kappa_1,\kappa_2,\kappa_3)$ is a three-dimensional real vector, and the components of the Pauli matrix vector σ are given by

$$\sigma_1 = \begin{bmatrix} 0 & 1 \\ 1 & 0 \end{bmatrix}, \quad \sigma_2 = \begin{bmatrix} 0 & -i \\ i & 0 \end{bmatrix}, \quad \sigma_3 = \begin{bmatrix} 1 & 0 \\ 0 & -1 \end{bmatrix}. \tag{A11}$$

The s evolution operator $u(s,s_0)$ of the equation of motion [Eq. (A9)] relates an initial state $|e(s_0)\rangle$ with a final state at some $s>s_0$:

$$|e(s)\rangle = u(s,s_0)|e(s_0)\rangle. \tag{A12}$$

It can be expressed as

$$u(s,s_0) = \lim_{N\to\infty}\prod_{n=1}^{N}\exp\left[i\frac{\Delta s}{N}\mathcal{K}(s_n)\right], \tag{A13}$$

where $\Delta s=s-s_0$, and $s_n=s_0+n\Delta s/N$. For a finite N the above expression can be used as a numerical approximation of $u(s,s_0)$. For calculating the exponential terms in Eq. (A13) it is useful to employ the following identity:

$$\exp(ix\mathcal{K}) = \exp(ik_0x)[I\cos(\alpha x) + i\hat{\kappa}\cdot\sigma\sin(\alpha x)], \tag{A14}$$

where the notation of Eq. (A10) is used, and $\kappa=\hat{\kappa}\alpha$ where $\hat{\kappa}$ is a unit vector and $\alpha=|\kappa|$.

The normalized SOP $|e\rangle$ can be represented as a point on the Bloch sphere indicating the expectation value of the Pauli spin vector matrix, namely,

$$\mathbf{P} = \langle e|\sigma|e\rangle. \tag{A15}$$

APPENDIX B: THE ADIABATIC CASE

To establish notation we review below the main results of Ref. 24. Consider the differential equation

$$\frac{\mathrm{d}}{\mathrm{d}s}|\psi\rangle = i\mathcal{K}|\psi\rangle, \tag{B1}$$

where $|\psi\rangle$ represents an N-dimensional column vector and $\mathcal{K}=\mathcal{K}(s)$ is an $N\times N$ Hermitian matrix. For any given value of s the Hermitian matrix $\mathcal{K}(s)$ has a set of orthonormal eigenvectors

$$\mathcal{K}|n(s)\rangle = K_n(s)|n(s)\rangle, \tag{B2}$$

where $n=1,2,\ldots,N$ and

$$\langle n(s)|m(s)\rangle = \delta_{nm}. \tag{B3}$$

The solution can be expanded as follows:

$$|\psi\rangle = \sum_n a_n(s)\exp\left[i\int_0^s \mathrm{d}s' K_n(s')\right]|n(s)\rangle. \tag{B4}$$

Substituting in Eq. (B1) yields

$$\dot{a}_m(s) = -\sum_n a_n(s)\exp\left\{i\int_0^s \mathrm{d}s'[K_n(s')-K_m(s')]\right\} \times\langle m(s)|\dot{n}(s)\rangle, \tag{B5}$$

where the upper dot represents a derivative with respect to s. The off-diagonal terms, given by

$$\langle m(s)|\dot{n}(s)\rangle = \frac{\langle m(s)|\dot{\mathcal{K}}|n(s)\rangle}{K_n(s)-K_m}, \tag{B6}$$

where $m\neq n$, are neglected in the adiabatic approximation. The resulting decoupled set of equations are easily solved:

$$a_m(s) = a_m(0)\exp(i\gamma_m), \tag{B7}$$

where the real phase γ_m is given by

$$\gamma_m = i\int_0^s \mathrm{d}s'\langle m(s')|\dot{m}(s')\rangle. \tag{B8}$$

Consider now the two-dimensional case $N=2$. Using the notation of Eq. (A10) and the notation $\kappa=\hat{\kappa}\alpha$, where $\hat{\kappa}$ is a unit vector, given in spherical coordinates by

$$\hat{\kappa} = (\cos\varphi\sin\theta, \sin\varphi\sin\theta, \cos\theta), \tag{B9}$$

one finds

$$\mathcal{K} = k_0 I + \alpha\begin{bmatrix} \cos\theta & \sin\theta\exp(-i\varphi) \\ \sin\theta\exp(i\varphi) & -\cos\theta \end{bmatrix}. \tag{B10}$$

The orthonormal eigenvectors are chosen to be

$$|\uparrow\rangle = \begin{bmatrix} \cos\frac{\theta}{2}\exp\left(-\frac{i\varphi}{2}\right) \\ \sin\frac{\theta}{2}\exp\left(\frac{i\varphi}{2}\right) \end{bmatrix}, \quad |\downarrow\rangle = \begin{bmatrix} -\sin\frac{\theta}{2}\exp\left(-\frac{i\varphi}{2}\right) \\ \cos\frac{\theta}{2}\exp\left(\frac{i\varphi}{2}\right) \end{bmatrix}, \tag{B11}$$

and the following holds: $\langle\uparrow|\uparrow\rangle=\langle\downarrow|\downarrow\rangle=1$, $\langle\uparrow|\downarrow\rangle=0$, and

$$\mathcal{K}|\uparrow\rangle = (k_0 + \alpha)|\uparrow\rangle, \tag{B12}$$

$$\mathcal{K}|\downarrow\rangle = (k_0 - \alpha)|\downarrow\rangle. \tag{B13}$$

The eigenstates $|n\rangle$ (where $n \in \{\uparrow, \downarrow\}$) are independent of k_0, thus

$$\gamma_m = i\int_{s_1}^{s_2} \mathrm{d}s\langle m(s)|\dot{m}(s)\rangle = i\int_{\kappa_1}^{\kappa_2} \mathrm{d}\kappa \cdot \langle m(\kappa)|\nabla_\kappa|m(\kappa)\rangle. \tag{B14}$$

Using the expression for a gradient in spherical coordinates, one finds

$$\langle\uparrow|\nabla_\kappa|\uparrow\rangle = -\frac{i\hat{\varphi}}{2\alpha}\cot\theta, \tag{B15}$$

$$\langle\downarrow|\nabla_\kappa|\downarrow\rangle = -\frac{i\hat{\varphi}}{2\alpha}\cot\theta. \tag{B16}$$

For the case of a close path, Stock's theorem can be used to express the integral in terms of a surface integral over the surface bounded by the close curve $\kappa(s)$:

$$\gamma_m = i\oint \mathrm{d}\kappa \cdot \langle m|\nabla_\kappa|m\rangle = i\int_S \mathrm{d}\mathbf{a} \cdot (\nabla \times \langle m|\nabla_\kappa|m\rangle). \tag{B17}$$

Expressing the curl operator in spherical coordinates, one finds

$$\nabla \times \langle\uparrow|\nabla_\kappa|\uparrow\rangle = \frac{i}{2}\frac{\kappa}{|\kappa|^3}, \tag{B18}$$

$$\nabla \times \langle\downarrow|\nabla_\kappa|\downarrow\rangle = -\frac{i}{2}\frac{\kappa}{|\kappa|^3}, \tag{B19}$$

$$\gamma_\uparrow = -\frac{1}{2}\int_S \mathrm{d}\mathbf{a} \cdot \frac{\kappa}{|\kappa|^3} = -\frac{1}{2}\Omega, \tag{B20}$$

$$\gamma_\downarrow = \frac{1}{2}\int_S \mathrm{d}\mathbf{a} \cdot \frac{\kappa}{|\kappa|^3} = \frac{1}{2}\Omega, \tag{B21}$$

where Ω is the solid angle subtended by the close path $\kappa(s)$ as seen from the origin. Because of the geometric nature of the last result, the phase factors $\gamma_\uparrow$ and $\gamma_\downarrow$ are called geometric phases. Thus

$$|\psi(s)\rangle = \begin{bmatrix} \exp(i\delta_\uparrow) & 0 \\ 0 & \exp(i\delta_\downarrow) \end{bmatrix}|\psi(0)\rangle, \tag{B22}$$

where

$$\delta_\uparrow = -\frac{\Omega}{2} + \int_0^s \mathrm{d}s'[k_0(s') + \alpha(s')], \tag{B23}$$

$$\delta_\downarrow = \frac{\Omega}{2} + \int_0^s \mathrm{d}s'[k_0(s') - \alpha(s')]. \tag{B24}$$

APPENDIX C: ZENER TRANSITIONS

The set of equations (B5) for the two-dimensional case of $N=2$ can be written in a matrix form as follows:

$$\frac{\mathrm{d}}{\mathrm{d}s}\begin{bmatrix} a_\uparrow \\ a_\downarrow \end{bmatrix} = \begin{bmatrix} -\langle\uparrow|\dot{\uparrow}\rangle & -\exp(i\beta)\langle\uparrow|\dot{\downarrow}\rangle \\ -\exp(-i\beta)\langle\downarrow|\dot{\uparrow}\rangle & -\langle\downarrow|\dot{\downarrow}\rangle \end{bmatrix}\begin{bmatrix} a_\uparrow \\ a_\downarrow \end{bmatrix}, \tag{C1}$$

where

$$\beta(s) = \int_0^s \mathrm{d}s'[K_\downarrow(s') - K_\uparrow(s')] = -2\int_0^s \mathrm{d}s'|\kappa|. \tag{C2}$$

In the adiabatic limit the off-diagonal matrix elements are considered negligibly small, and consequently no transitions between the adiabatic states occur. To calculate the transition probability to lowest order we consider the off-diagonal elements as a perturbation.[32] The solution of the unperturbed problem is given by

$$a_\downarrow(s) = a_\downarrow(0)\exp(i\gamma_\downarrow), \tag{C3}$$

$$a_\uparrow(s) = a_\uparrow(0)\exp(i\gamma_\uparrow). \tag{C4}$$

Assuming at some initial point s_0 that the system was in the $|\downarrow\rangle$ state, we wish to calculate the probability to find the system in the $|\uparrow\rangle$ state at $s > s_0$. Lowest-order correction is obtained by substituting the unperturbed solution in Eq. (C1):

$$\frac{\mathrm{d}}{\mathrm{d}s}a_\uparrow = -a_\downarrow(0)\exp[i(\beta + \gamma_\downarrow)]\langle\uparrow|\dot{\downarrow}\rangle. \tag{C5}$$

Thus, to lowest order, the transition probability is given by

$$p_z = \left|\int_{s_0}^s \mathrm{d}s' \exp[i(\beta + \gamma_\downarrow)]\langle\uparrow|\dot{\downarrow}\rangle\right|^2. \tag{C6}$$

Consider the case where $\kappa = \alpha(\cos\varphi\sin\theta, \sin\varphi\sin\theta, \cos\theta)$ is planar with $\varphi = \text{const}$. Using Eqs. (B11),

$$|\dot{\downarrow}\rangle = -\frac{\dot{\theta}}{2}|\uparrow\rangle; \tag{C7}$$

thus

$$\langle\uparrow|\dot{\downarrow}\rangle = -\frac{\dot{\theta}}{2}. \tag{C8}$$

Similarly

$$\langle\downarrow|\dot{\downarrow}\rangle = 0, \tag{C9}$$

thus $\gamma_\downarrow = 0$. Using the above results,

$$p_z = \frac{1}{4}\left|\int \mathrm{d}\theta \exp(i\zeta)\right|^2, \tag{C10}$$

where

$$\zeta(\theta) = -2\int_0^{s(\theta)} \mathrm{d}s'|\kappa|. \tag{C11}$$

1. Case Where $\kappa(s)$ Is a Half-Circle

Consider the case where $\mathcal{K}=\kappa\cdot\sigma$, where

$$\kappa(s)=\gamma(\sqrt{\Lambda^2-(\gamma s)^2},0,\gamma s). \tag{C12}$$

Here γ is a nonnegative real constant with dimensionality of 1/length, Λ is a nonnegative dimensionless real parameter, and $|s|<\Lambda/\gamma$.

The Zener transition probability is calculated for the case $\Lambda\gtrsim 1$ to lowest order in the adiabatic expansion. The following holds:

$$\cos\theta=\frac{\gamma s}{\Lambda}, \tag{C13}$$

and $|\kappa|=\gamma\Lambda$; thus

$$\zeta(\theta)=-2\int_0^{s(\theta)}\mathrm{d}s'|\kappa|=-2\Lambda^2\cos\theta, \tag{C14}$$

$$p_z=\frac{1}{4}\left|\int_{-\pi}^{0}\mathrm{d}\theta\exp(-2i\Lambda^2\cos\theta)\right|^2. \tag{C15}$$

Using the identity

$$\int_0^{\pi}\mathrm{d}\theta\exp(iz\cos\theta)=\pi J_0(z), \tag{C16}$$

one finds

$$p_z\simeq\frac{\pi^2}{4}J_0^2(2\Lambda^2)\quad(\text{for }\Lambda\gtrsim 1). \tag{C17}$$

Figure 5 shows an example of numerical integration of the equation of motion for the case of $\Lambda=5$. Figure 5(a) shows the half-circle $\kappa(s)$ curve and Fig. 5(b) shows the evolution of the polarization vector on the Bloch sphere. Figure 6 shows a numerical calculation of the Zener transition probability p_z as a function of the parameter Λ. As can be seen in Fig. 6, p_z vanishes for a series of points we denote as Λ_n ($n=1,2,3\ldots$). The first zero of p_z is at $\Lambda_1=1.022$. Note, however, that even though p_z vanishes at the points Λ_n, the evolution becomes truly adiabatic only when $\Lambda\gg 1$.

Comparing relation (C17) with the numerical solution seen in Fig. 6 shows, as expected, good agreement for $\Lambda\gtrsim 1$. For the range $0\leqslant\Lambda\lesssim 1$, however, we find that the following can serve as a good approximation:

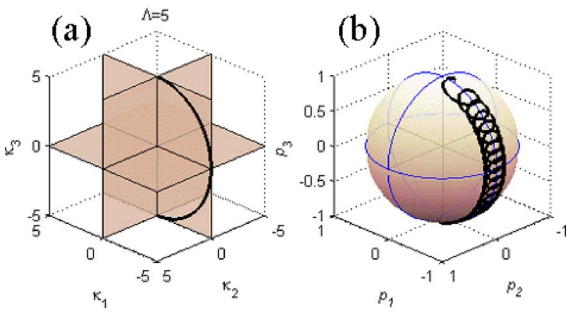

Fig. 5. (Color online) Example of numerical integration of the equation of motion for the case of $\Lambda=5$. (a) Curve $\kappa(s)$; (b) the evolution of the polarization vector $\mathbf{p}(s)$ on the Bloch sphere.

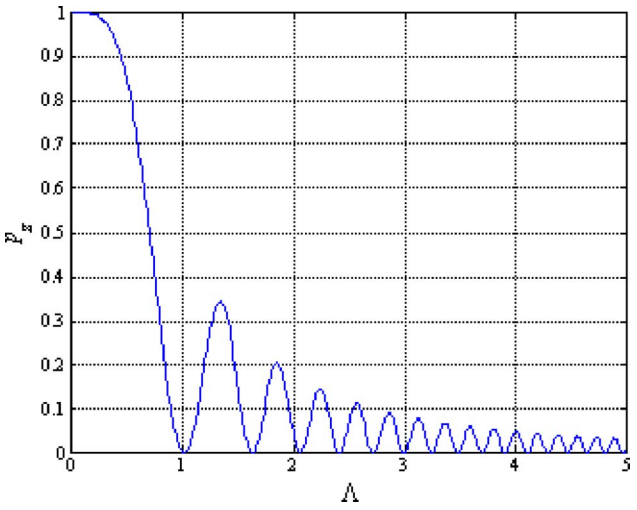

Fig. 6. (Color online) Zener probability p_z versus the parameter Λ calculated numerically.

$$p_z\simeq J_0^2\left(\frac{\pi\Lambda^2}{\sqrt{2}}\right)\quad(\text{for }0\leqslant\Lambda\lesssim 1). \tag{C18}$$

2. Case Where $\kappa(s)$ Is a Straight Line

We calculate p_z for the case $\mathcal{K}=\kappa\cdot\sigma$, where $\kappa(s)$ is a straight line:

$$\kappa(s)=\Delta(0,1,\gamma s), \tag{C19}$$

where Δ and γ are real constants independent of s.

For the present case one has

$$\zeta(s)=-2\Delta\int_0^s\mathrm{d}s'\sqrt{1+(\gamma s')^2}=-\frac{\Delta}{\gamma}[\gamma s\sqrt{1+(\gamma s)^2}\sinh^{-1}(\gamma s)], \tag{C20}$$

$$-\frac{1}{2}\int_{\pi}^{0}\mathrm{d}\theta\exp(i\zeta)=\frac{1}{2}\int_{-\infty}^{\infty}\frac{1}{\cosh z}\times\exp\left[-i\frac{\Delta}{\gamma}\left(\frac{1}{2}\sinh 2z+z\right)\right]\mathrm{d}z. \tag{C21}$$

In the limit $\Delta/\gamma\to\infty$ the phase oscillates rapidly and consequently $p_z\to 0$. The stationary phase points z_n in the complex plane are found from the condition

$$0=\frac{\mathrm{d}}{\mathrm{d}z}\left(\frac{1}{2}\sinh 2z+z\right)=\cosh 2z+1; \tag{C22}$$

thus

$$z_n=i\pi\left(n+\frac{1}{2}\right), \tag{C23}$$

where n is an integer. Note, however, that the term $1/\cosh z$ has poles at the same points. Using Cauchy's theorem the path of integration can be deformed to pass close to the point $z_{-1}=-i\pi/2$. Since the pole at z_{-1} is a simple one, the principal value of the integral exists. To avoid passing through the pole at z_{-1}, a trajectory forming

a half-circle above the pole with radius ϵ is chosen as $\epsilon \to 0$. This subsection gives the dominant contribution, which is $i\pi R$, where R is the residue at the pole. Thus one finds

$$\left| \frac{1}{2} \int_{\pi}^{0} d\theta \exp(i\zeta) \right| \simeq \exp\left(-\frac{\pi}{2} \frac{\Delta}{\gamma} \right). \tag{C24}$$

The prefactor in front of the exponent is determined by requiring $p_z = 1$ in the limit of $\Delta \ll \gamma$, thus

$$p_z \simeq \exp\left(-\pi \frac{\Delta}{\gamma} \right). \tag{C25}$$

ACKNOWLEDGMENTS

The author especially thanks Avishai Eyal for many helpful conversations and invaluable suggestions. Also, a discussion with Steve Lipson is gratefully acknowledged.

The author's e-mail address is eyal@ee.technion.ac.il.

REFERENCES

1. A. Yariv, "Universal relations for coupling of optical power between microresonators and dielectric waveguides," Electron. Lett. **36**, 321–322 (2000).
2. A. Yariv, "Critical coupling and its control in optical waveguide-ring resonator systems," IEEE Photon. Technol. Lett. **14**, 483–485 (2002).
3. J. M. Choi, R. K. Lee, and A. Yariv, "Control of critical coupling in a ring resonator–fiber configuration: application to wavelength-selective switching, modulation, amplification, and oscillation," Opt. Lett. **26**, 1236–1238 (2001).
4. V. M. Menon, W. Tong, and S. R. Forrest, "Control of quality factor and critical coupling in microring resonators through integration of a semiconductor optical amplifier," IEEE Photon. Technol. Lett. **16**, 1343–1345 (2004).
5. Yu. A. Kravtsov and Yu. I. Orlov, *Geometrical Optics of Inhomogeneous Media* (Springer-Verlag, 1990).
6. S. Pancharatnam, "Generalized theory of interference, and its applications," Proc. Indian Acad. Sci. Sect. A **44**, 247–262 (1956).
7. J. N. Ross, "The rotation of the polarization in low birefringence monomode optical fibers due to geometric effects," Opt. Quantum Electron. **16**, 455–461 (1984).
8. A. Tomita and R. Y. Chiao, "Observation of Berry's topological phase by use of an optical fiber," Phys. Rev. Lett. **57**, 937–940 (1986).
9. F. D. M. Haldane, "Path dependence of the geometric rotation of polarization in optical fibers," Opt. Lett. **11**, 730–732 (1986).
10. M. V. Berry, "Interpreting the anholonomy of coiled light," Nature **326**, 277–278 (1987).
11. M. V. Berry, "The adiabatic phase and Pancharatnam's phase for polarized light," J. Mod. Opt. **34**, 1401–1407 (1987).
12. N. J. Frigo, "A generalized geometrical representation of coupled mode theory," IEEE J. Quantum Electron. **QE-22**, 2131–2140 (1986).
13. M. Kugler and S. Shtrikman, "Berry's phase, locally inertial frames, and classical analogues," Phys. Rev. D **37**, 934–937 (1988).
14. H. Jiao, S. R. Wilkinson, and R. Y. Chiao, "Two topological phases in optics by means of a nonplanar Mach–Zehnder interferometer," Phys. Rev. A **39**, 3475–3486 (1989).
15. S. G. Lipson, "Berry's phase in optical interferometry: a simple derivation," Opt. Lett. **15**, 154–155 (1990).
16. O. J. Kwon, H. T. Lee, S. B. Lee, and S. S. Choi, "Observation of a topological phase in a noncyclic case by use of a half-turn optical fiber," Opt. Lett. **16**, 223–225 (1991).
17. L. H. Ryder, "The optical Berry phase and the Gauss–Bonnet theorem," Eur. J. Phys. **12**, 15–18 (1991).
18. C. R. Menyuk and P. K. A. Wai, "Polarization evolution and dispersion in fibers with spatially varying birefringence," J. Opt. Soc. Am. B **11**, 1288–1296 (1994).
19. C. S. Brown and A. E. Bak, "Unified formalism for polarization optics with application to polarimetry on a twisted optical fiber," Opt. Eng. (Bellingham) **34**, 1625–1635 (1995).
20. E. M. Frins and W. Dultz, "Direct observation of Berry's topological phase by using an optical fiber ring interferometer," Opt. Commun. **136**, 354–356 (1997).
21. F. Wassmann and A. Ankiewicz, "Berry's phase analysis of polarization rotation in helicoidal fibers," Appl. Opt. **37**, 3902–3911 (1998).
22. P. Senthilkumaran, B. Culshaw, and G. Thursby, "Fiber-optic Sagnac interferometer for the observation of Berry's topological phase," J. Opt. Soc. Am. B **17**, 1914–1919 (2000).
23. P. Senthilkumaran, G. Thursby, and B. Culshaw, "Fiber-optic tunable loop mirror using Berry's geometric phase," Opt. Lett. **25**, 533–535 (2000).
24. M. V. Berry, "Quantal phase-factors accompanying adiabatic changes," Proc. R. Soc. London Ser. A **392**, 45–57 (1984).
25. R. Bhandari, "SU(2) phase jumps and geometric phases," Phys. Lett. A **157**, 221–225 (1991).
26. R. Bhandari, "Interferometry without beam-splitter—a sensitive technique for spinor phases," Phys. Lett. A **180**, 21–24 (1993).
27. R. Bhandari, "Polarization of light and topological phases," Phys. Rep. **281**, 2–64 (1997).
28. H. Schmitzer, S. Klein, and W. Dultz, "Nonlinearity of Pancharatnam's topological phase," Phys. Rev. Lett. **71**, 1530–1533 (1993).
29. B. Hils, W. Dultz, and W. Martienssen, "Nonlinearity of Pancharatnam's geometric phase in polarizing interferometers," Phys. Rev. E **60**, 2322–2329 (1999).
30. S. P. Tewari, V. S. Ashoka, and M. S. Ramana, "A 4-arm Sagnac interferometric switch," Opt. Commun. **120**, 235–238 (1995).
31. Q. Li, L. F. Gong, Y. H. Gao, and Y. L. Chen, "Experimental observation of the nonlinearity of the Pancharatnam phase with a Michelson interferometer," Opt. Commun. **169**, 17–22 (1999).
32. Y. Lyanda-Geller, "Topological transitions in Berry's phase interference effects," Phys. Rev. Lett. **71**, 657–661 (1993).
33. K. P. Marzlin and B. C. Sanders, "Inconsistency in the application of the adiabatic theorem," Phys. Rev. Lett. **93**, 160408 (2004).
34. E. Buks, "Upper bound imposed upon responsivity of optical modulators," arxiv.org/abs/quant-ph/0510119.
35. A. Simon and R. Ulrich, "Evolution of polarization along a single-mode fiber," Appl. Phys. Lett. **31**, 517–520 (1977).
36. R. Ulrich and A. Simon, "Polarization optics of twisted single-mode fibers," Appl. Opt. **18**, 2241–2251 (1979).
37. C. H. Tang, "An orthogonal coordinate system for curved pipes (correspondence)," IEEE Trans. Microwave Theory Tech. **MTT-18**, 69 (1970).